Tuning the Skyrmion Hall Effect via Engineering of Spin-Orbit Interaction

Collins Ashu Akosa, Hang Li, Gen Tatara, and Oleg A. Tretiakov

Phys. Rev. Applied **12**, 054032 — Published 13 November 2019

DOI: 10.1103/PhysRevApplied.12.054032

Tuning skyrmion Hall effect via engineering of spin-orbit interaction

Collins Ashu Akosa[1,2,*] Hang Li[3], Gen Tatara[1,4], and Oleg A. Tretiakov[5†]
[1] *RIKEN Center for Emergent Matter Science (CEMS), 2-1 Hirosawa, Wako, Saitama 351-0198, Japan*
[2] *Department of Theoretical and Applied Physics, African University of Science and Technology (AUST), Km 10 Airport Road, Galadimawa, Abuja F.C.T, Nigeria*
[3] *Institute for Computational Materials Science, School of Physics and Electronics, Henan University, Kaifeng 475004, China*
[4] *RIKEN Cluster for Pioneering Research (CPR), 2-1 Hirosawa, Wako, Saitama, 351-0198 Japan and*
[5] *School of Physics, The University of New South Wales, Sydney 2052, Australia*
(Dated: October 28, 2019)

We demonstrate that the Magnus force acting on magnetic skyrmions can be efficiently tuned via modulation of the strength of spin-orbit interaction. We show that the skyrmion Hall effect, which is a direct consequence of the non-vanishing Magnus force on the magnetic structure can be suppressed in certain limits. Our calculations show that the emergent magnetic fields in the presence of spin-orbit coupling (SOC) renormalize the Lorentz force on itinerant electrons and thus influence the topological transport. In particular, we show that for a Néel-type skyrmion and Bloch-type antiskyrmion, the skyrmion Hall effect (SkHE) can vanish by tuning appropriately the strength of Rashba and Dresselhaus SOCs, respectively. Our results open up alternative directions to explore in a bid to overcoming the parasitic and undesirable SkHE for spintronic applications.

I. INTRODUCTION

Over the last decade, spintronic research interest has switched towards a novel direction called *spin-orbitronics* that exploits the relativistic coupling of electron's spin to its orbit to create new and intriguing effects and materials [1–3]. It turns out that spin-orbit interaction is very crucial in effects related to the efficient conversion of charge to spin current [4, 5], that is essential for spintronic applications. The former has been largely exploited for the creation of a novel class of topological materials such as chiral domain walls and magnetic skyrmions with enhanced thermal stability, low critical currents and smaller sizes. Therefore, spin-orbit related effects open up promising directions to create, manipulate, and detect spin currents for spintronic applications.

In magnetic materials with broken inversion symmetry, an atom with strong SOC can mediate an antisymmetric exchange interaction called the Dzyaloshinskii-Moriya interaction (DMI), that favors the non-collinear alignments of atomic spins [6, 7]. In such materials, the competition between the DMI and other magnetic interactions notably, the exchange (that favors collinear alignment of atomic spins) is essential for the stabilization of exotic magnetic states such as helimagnets [8] and magnetic skyrmions [9]. The later have been widely projected as a viable contender for information carriers in the next-generation data storage and spin logic devices due to their small spatial extent, high topological protection, and efficient current-induced manipulation that allows for robust, energy-efficient, and ultra-high density spintronic applications [10, 11]. However, the integration of ferromagnetic skyrmions in such applications is hindered by the undesirable SkHE, a transverse motion to the direction of current flow [12, 13].

To overcome this parasitic effect, several proposals have been put forward such as, the use of antiferromagnetic skyrmions [14–17], edge

* collins.akosa@riken.jp
† o.tretiakov@unsw.edu.au

repulsion [18], magnetic bilayer-skyrmion [19], skyrmionium [20–25], antiskyrmions [26, 27], and via spin current partially polarized along the direction of applied current [28]. These proposals focus on suppressing the inherent Magnus force in these systems, while little attention has been paid to understanding its source, i.e., the nature of the texture-induced emergent magnetic field. Moreover, since the stabilization of topological magnetic textures such as skyrmions, usually requires strong SOC, it is important to investigate the effect of the latter on these fictitious electromagnetic fields. Indeed, recent studies showed that SOC induces additional fictitious electric field that manifests itself as spin-motive force [33, 34] on the itinerant electrons and gives raise to charge current [35] and chiral damping [36]. However, the effect of the SOC-induced emergent magnetic field on the conduction electrons has more or less been overlooked.

In this paper, we provide a theoretical framework that takes into account these fictitious magnetic fields and elucidate their impact on the topological transport inherent to magnetic skyrmions. We demonstrate that the SkHE, which is a direct consequence of a non-vanishing Magnus force on the magnetic structure can be efficiently tuned via modulation of the strength of the spin-orbit interaction. In particular, we show that for a Néel-type skyrmion and Bloch-type antiskyrmion, the SkHE can be tuned to zero via the modulation of the strength of the Rashba SOC (RSOC) and Dresselhaus (DSOC), respectively. Our results opens up alternative directions to overcoming the parasitic and undesirable SkHE in ferromagnetic skyrmions.

II. THEORETICAL MODEL

It is known that DSOC stabilizes Bloch-type skyrmions [39–41], while RSOC stabilizes Néel-type skyrmions [42, 43]. However, recent realization of Bloch-type skyrmions in Rashba metals [44, 45] motivates us here to consider an interplay of both types of SOC in a two-dimensional skyrmionic system described by the Hamiltonian

$$\hat{\mathcal{H}} = \frac{\hat{\boldsymbol{p}}^2}{2m^*} + J\boldsymbol{m}(\boldsymbol{r}) \cdot \hat{\boldsymbol{\sigma}} + \hat{\mathcal{H}}_R + \hat{\mathcal{H}}_D, \qquad (1)$$

where m^* is the effective mass of electrons, $\hat{\boldsymbol{p}}$ is the momentum operator, J is the exchange interaction between the local moments in the direction of the unit vector $\boldsymbol{m}$ and spins of itinerant electrons given by vector of Pauli matrices $\hat{\boldsymbol{\sigma}}$. The terms $\mathcal{H}_R = \beta_R(\sigma_y p_x - \sigma_x p_y)/\hbar$ and $\mathcal{H}_D = \beta_D(\sigma_x p_x - \sigma_y p_y)/\hbar$ describe the RSOC and DSOC, respectively. Furthermore, we consider J to be the dominant interaction compared to the SOCs, and since our considerations are based two-dimensional systems with strong confinement along $\boldsymbol{e}_z$, the cubic-DSOC contribution is assumed to be small and negligible [37, 38]. To keep our analysis trackable, we consider an isolated skyrmion (antiskyrmion) with analytical ansatz without loss of generality given in spherical coordinates

$$\boldsymbol{m}(\boldsymbol{r}) = \big(\cos\Phi\sin\theta, \sin\Phi\sin\theta, \cos\theta\big), \qquad (2)$$

where the azimuthal angle is given as

$$\Phi(x,y) = q\,\mathrm{Arg}\,(x,y) + \gamma_c, \qquad (3)$$

where $q = \pm 1$ is the *vorticity*, i.e., $q = +1$ for *skyrmions* and $q = -1$ for *antiskyrmions*, and c is the *heliticity* such that $\gamma_c = 0$ or π for Néel-type and $\gamma_c = \pm\pi/2$ for Bloch-type skyrmions and antiskyrmions. To provide a very general analysis, we consider the radial angle $\theta(r)$ with properties [46]

$$\cos\theta\big(r\big)_{r\to 0} = -\cos\theta\big(r\big)_{r\to R} = p, \qquad (4)$$

and

$$\sin\theta\big(r\big)_{r\to 0} = \sin\theta\big(r\big)_{r\to R} = 0, \qquad (5)$$

where $R \gg r_s$, r_s being the skyrmion radius, $p = \pm 1$ is the *polarity* that defines the orientation of the skyrmion's core. In this representation, the topological charge Q of the magnetic solitons is given by $Q = pq$ [47]. Before we proceed, we note that our theoretical analysis is general and does not depend on any particular ansatz that satisfy Eqs. (3), (4) and (5). However, for our numerical calculations, we consider the radial angle given as $\theta(r) = \pi(3-p)/2 + 4\tan^{-1}(e^{r/r_s})$.

III. ANALYTICAL RESULTS

It is well established that when itinerant electrons traverse a smooth and slowly varying magnetic texture, $\boldsymbol{m}(\boldsymbol{r})$, there is a reorientation of their spins to follow the direction of local magnetization. This process gives raise to *fictitious* electromagnetic fields that act on the itinerant electrons. The emergent electrodynamics resulting from the system described by Eq. (1) is derived following the standard approach, i.e., the exchange term is diagonalized via a unitary transformation $\hat{U} = \boldsymbol{n} \cdot \hat{\boldsymbol{\sigma}}$, where $\boldsymbol{n} = \big(\cos\Phi \sin(\theta/2), \sin\Phi \sin(\theta/2), \cos(\theta/2)\big)$ in the spin-space [48, 49]. The end result being that itinerant electrons in the transformed frame are subjected to a uniform ferromagnetic state and weakly coupled to the *spin gauge fields* given as

$$\mathcal{A}_{\eta,\mu} = A^{\alpha}_{\eta,\mu} \cdot \sigma^{\alpha} = A^{z}_{\eta,\mu} \cdot \sigma^{z} + \boldsymbol{A}^{\perp}_{\eta,\mu} \cdot \boldsymbol{\sigma}^{\perp}, \quad (6)$$

where $\eta = s, R, D$ for the texture, Rashba and Dresselhaus induced gauge fields, respectively, α and μ represent the spin and real-space indices, respectively, $\boldsymbol{A}^{\perp}_{\eta,\mu} = (A^{x}_{\eta,\mu}, A^{y}_{\eta,\mu}, 0)$, and $\boldsymbol{\sigma}^{\perp} = (\sigma^x, \sigma^y, 0)$. We ignore the off-diagonal component $\boldsymbol{A}^{\perp}_{\eta,\mu}$ that describe nonadiabatic processes which is important in the nonadiabatic regime of weak exchange and/or sharp magnetic textures [50–53] typical in dilute magnetic semiconductors [54]. In this study, we focus on the $A^{z}_{\eta,\mu}$ component which is diagonal and describe adiabatic processes that preserve the spin state in all parameter space considered. The origin of the spin gauge fields given by Eq. (6) represented by the subscript η include contributions: (i) due to the magnetic texture $\boldsymbol{A}^{z}_{s}$, (ii) as a result of an interplay between RSOC and the magnetic texture $\boldsymbol{A}^{z}_{R}$, and (iii) interplay between DSOC and the magnetic texture $\boldsymbol{A}^{z}_{D}$ given by [36]

$$\boldsymbol{A}^{z}_{s} = \mp\frac{\hbar}{2e}\big(1 - \cos\theta\big)\boldsymbol{\nabla}\Phi, \quad (7a)$$

$$\boldsymbol{A}^{z}_{R} = \mp\frac{\hbar}{2e}\frac{\big(m_y \boldsymbol{e}_x - m_x \boldsymbol{e}_y\big)}{\lambda_R}, \quad (7b)$$

$$\boldsymbol{A}^{z}_{D} = \mp\frac{\hbar}{2e}\frac{\big(m_x \boldsymbol{e}_x - m_y \boldsymbol{e}_y\big)}{\lambda_D}, \quad (7c)$$

where $\mp$ represents the spin projections i.e., $-1(+1)$ for spin-up(down) [55] and $\lambda_{R(D)} = \hbar^2/2m^*\beta_{R(D)}$ is the characteristic length scale of the RSOC (DSOC). While the previous studies have focused on the effect of the SOC-induced emergent electric field on the itinerant electrons (spin-motive force), here, we focus on the effect of the corresponding emergent magnetic field on the itinerant electrons (Lorentz force) which are calculated from the spin gauge fields using

$$\boldsymbol{B}_{\eta} = \boldsymbol{\nabla} \times \boldsymbol{A}^{z}_{\eta}, \quad (8)$$

to obtain

$$B_s = \mp\frac{\hbar}{2e}\big([\partial_x \boldsymbol{m} \times \partial_y \boldsymbol{m}] \cdot \boldsymbol{m}\big), \quad (9a)$$

$$B_R = \pm\frac{\hbar}{2e}\frac{\big(\partial_x m_x + \partial_y m_y\big)}{\lambda_R} + \mathcal{O}(\beta_R^2), \quad (9b)$$

$$B_D = \pm\frac{\hbar}{2e}\frac{\big(\partial_x m_y + \partial_y m_x\big)}{\lambda_D} + \mathcal{O}(\beta_D^2). \quad (9c)$$

It turns out that $\boldsymbol{B}_s$ and $\boldsymbol{B}_R$ in Eq. (9) act in the opposite directions for Néel-type skyrmions as illustrated in Fig. 1. The direct consequence of this fact is that the electrons traversing an array of Néel-type skyrmions in the positive **x**-direction, experience two opposite fictitious magnetic fields: $\boldsymbol{B}_s$ in the positive **z**-direction that tends to deflect the electrons in the positive **y**-direction and $\boldsymbol{B}_R$ in the negative **z**-direction that tends to deflect the electrons in the negative **y**-direction. Since $\boldsymbol{B}_R$ has two free parameters r_s and λ_R, by tuning them, one can realize a condition when $\boldsymbol{B}_R$ completely cancels out $\boldsymbol{B}_s$ [i.e. $\lambda_R \approx r_s/2$ as given in Eq. (12)]. In this case, the transverse *Lorentz force* acting on electrons transversing the skyrmions is completely suppressed, or equivalently the *Magnus force* on the magnetic structure is vanishing.

To gain more insight into the physics originating from the interplay of the different contributions to emergent magnetic fields given by Eq. (9), we consider a discrete square system of size $101 \times 101 a_0^2$, with the equilibrium skyrmion radius $r_s = 12a_0$, where $a_0 = 0.3$ nm is the lattice constant. Furthermore, we take the effective mass of electrons $m^* = 0.4m_0$, where m_0

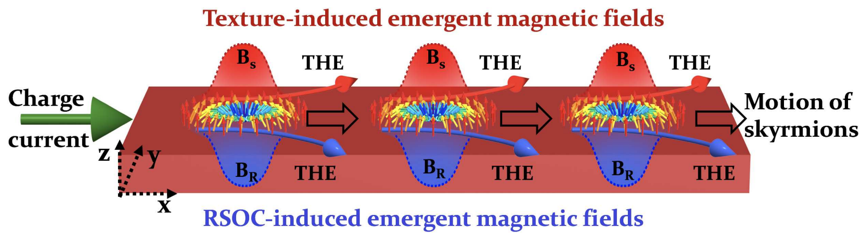

FIG. 1. Schematic illustration of the current-driven motion of *Néel-type skyrmions* array in the presence of SOC. Fields $\boldsymbol{B}_s$ (red) and $\boldsymbol{B}_R$ (blue) act in opposite directions, leading to the topological Hall effect (THE) on traversing electrons also in opposite directions. As such, tuning $\boldsymbol{B}_R$ through the strength of the SOC can produce current-driven motion without skyrmion Hall effect (black arrows).

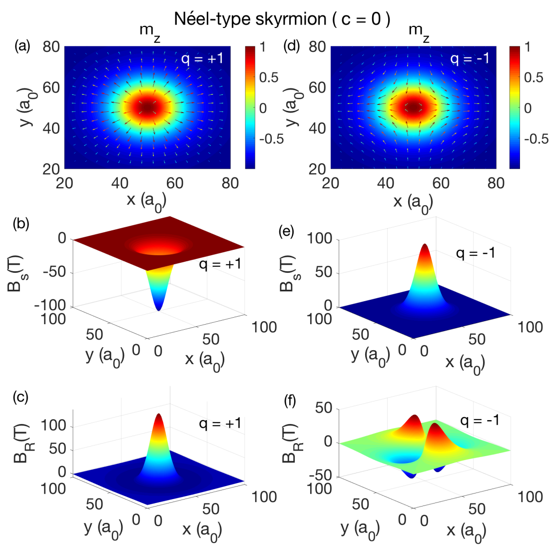

FIG. 2. Schematic diagram of the spatial magnetization profile for a Néel-type skyrmion (a) and antiskyrmion (b), and their corresponding emergent magnetic fields (c, e) and (d, f), respectively, in the presence of RSOC.

is the bare mass of electrons, and the RSOC strength $\beta_R = 2.5 \times 10^{-11}$eV m (equivalent to $\lambda_R = 3.8$ nm). Then we calculate the corresponding magnetic fields for different vorticities and helicities. In Fig. 2, the results for *Néel-type skyrmions* ($q = +1$) and *antiskyrmions* ($q = -1$) are shown with the magnetization profiles given by those presented in Figs. 2(a) and (d), respectively. We see that for *Néel-type skyrmions*, indeed, the fictitious magnetic fields $\boldsymbol{B}_s$ [c.f. Fig. 2(b)] and $\boldsymbol{B}_R$ [c.f. Fig. 2(c)] act in opposite directions such that, it is possible to achieve a current-driven motion without SkHE by tuning the strength of the RSOC. However, in the case of a *Néel antiskyrmion* as shown in Figs. 2(e) and (f), even though the transversing electrons experience these fictitious magnetic fields, the effect of $\boldsymbol{B}_R$ on its trajectory cancels out by symmetry [c.f. Fig. 2(f)]. As such, only $\boldsymbol{B}_s$ influences its trajectory leading to SkHE for current-driven motion.

Similar arguments can be used to explain the characteristics of Bloch-type *skyrmions* and *antiskyrmions* as shown in Fig. 3, with the magnetization profiles as depicted in Figs. 3(a) and (d), respectively. It turns out that unlike in the Néel-type case, the SOC-induced fictitious magnetic field $\boldsymbol{B}_D$, does not influence the trajectory of electrons traversing *Bloch-type skyrmions*, since the latter cancels out by symmetry [c.f. Fig. 3(c)]. As such the trajectory of traversing electrons are detected by $\boldsymbol{B}_s$ [c.f. Fig. 3(b)] leading to SkHE for current-driven motion. However, in the case of *Bloch-type antiskyrmions*, $\boldsymbol{B}_s$ [c.f. Fig. 3(e)] and $\boldsymbol{B}_D$ [c.f. Fig. 3(f)] act in the opposite directions and as a result, by tuning the strength of DSOC and/or the r_s via material engineering, it is possible to achieve a SkHE-free current-driven motion of Bloch antiskyrmions [i.e. $\lambda_D \approx r_s/2$ as given in

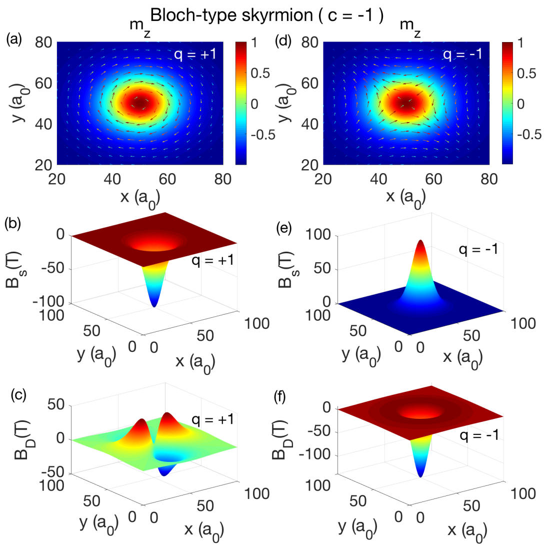

FIG. 3. Schematic diagram of the spatial magnetization profile for a Bloch-type skyrmion (a) and antiskyrmion (b), and their corresponding emergent magnetic fields (c, e) and (d, f), respectively, in the presence of DSOC.

Eq. (12)]. Therefore, our analysis shows that, depending on the vorticity and chirality of ferromagnetic solitons, it is possible to achieve a current-driven motion of the latter without SkHE via the engineering of the spin-orbit interaction in the system. Although the heuristic analysis presented above, captures the important physics, In what follows, we provide a more rigorous argument based on the average emergent magnetic field that electrons traversing magnetic skyrmions experience.

A straight forward calculation of emergent magnetic fields given in Eq. (9) using the general ansatz in Eqs. (3), (4) and (5) yields

$$B_s = \mp \frac{q\hbar}{2e}\frac{\mathrm{d}\theta}{\mathrm{d}r}\frac{\sin\theta}{r}, \tag{10a}$$

$$B_R = \pm \frac{\hbar}{2e\lambda_R}\left(\frac{\mathrm{d}\theta}{\mathrm{d}r}\cos\theta + q\frac{\sin\theta}{r}\right)\cos\Big(\Phi - q\Phi - \gamma_c\Big) + \mathcal{O}\Big(\beta_R^2\Big), \tag{10b}$$

$$B_D = \pm \frac{\hbar}{2e\lambda_D}\left(\frac{\mathrm{d}\theta}{\mathrm{d}r}\cos\theta - q\frac{\sin\theta}{r}\right)\sin\Big(\Phi + q\Phi - q\gamma_c\Big) + \mathcal{O}\Big(\beta_D^2\Big), \tag{10c}$$

from which the following inference is immediately drawn: (i) a Néel ($\gamma_c = 0$ or π) skyrmion ($q = +1$) in the present of RSOC experiences and equal but opposite emergent magnetic field as Bloch ($\gamma_c = -\pi/2$ or $\pi/2$) antiskyrmion ($q = -1$) in the present of DSOC. (ii) due to the symmetry of Φ as defined by Eq. (3), the spatial average of RSOC-induced emergent magnetic field for Néel antiskyrmions [c.f. Eq. (10b)] and DSOC-induced emergent magnetic field for Bloch antiskyrmions [c.f. Eq. (10c)] vanishes. Since we focus on the half-metallic and strong adiabatic regimes in which spin-flip processes are not relevant, the THE can be quantified by the average fictitious magnetic fields. However, we note that such description in the ballistic regime, especially in the weak exchange limit is subtle [50, 53]. The average fictitious magnetic fields are calculated as $\langle B_\eta \rangle_{\mathrm{av}} =$

$\int B_\eta \mathrm{d}^2\boldsymbol{r}/\int \mathrm{d}^2\boldsymbol{r}$ from Eq. (10), so that

$$\langle B_s\rangle_{\rm av} = \mp\frac{2pq\hbar}{eR^2}, \tag{11a}$$

$$\langle B_R\rangle_{\rm av} = \pm\frac{p\hbar(1+q)r_s}{2e\lambda_R R^2}\cos\gamma_c + \mathcal{O}(\beta_R^2), \tag{11b}$$

$$\langle B_D\rangle_{\rm av} = \pm\frac{p\hbar(1-q)r_s}{2e\lambda_D R^2}\sin\gamma_c + \mathcal{O}(\beta_D^2). \tag{11c}$$

We immediately deduce from Eq. (11) that up to the linear order in SOC, the average SOC-emergent magnetic field: (i) vanishes for Néel antiskyrmions [c.f. $q = -1$, in Eq. (11b)] and Bloch skyrmions [c.f. $q = +1$, in Eq. (11c)] (ii) is finite and is opposite to $\boldsymbol{B}_s$ for Néel skyrmions [c.f. $q = +1$, in Eq. (11b)] and Bloch antiskyrmions [c.f. $q = -1$, in Eq. (11c)]. As a result, since the topological Hall effect of itinerant electrons as they traverse magnetic skyrmions is governed by these average fictitious magnetic fields, we recover the conclusions discussed in our heuristic analysis above. Interestingly, these average additional fictitious magnetic fields are proportional to $\beta_{R,D} r_s$, and since the DMI has a subtle dependence on r_s [56, 57], but is proportional to the strength of the SOC [58, 59], one expects that the former should be at least dependent on the strength of the DMI in these systems. This theoretical prediction provides an interesting direction to explore to tune and potentially completely overcome this undesirable SkHE for spintronic applications.

To conclude this section, we deduce the critical value the SOC ($\alpha^c_{R(D)}$) [or equivalently $\lambda^c_{R(D)}$] for the complete cancellation of emergent magnetic field for Néel (Bloch) skyrmion (antiskyrmion) [c.f. calculated from Eq (11) by setting $\langle B_{R(D)}\rangle_{\rm av} = \langle B_s\rangle_{\rm av}$] as

$$\lambda^c_{R,D} \approx r_s/2. \tag{12}$$

Eq. (12) is very important and should act as a guide for material engineering of topological transport in magnetic solitons.

An interesting extension, which is however out of the scope of the present work, would be to directly investigate this effect via micromagnetic simulations. This is achievable via for example, taking into account the effect of the spin torques induced by the fictitious magnetic fields in Eq. (9). Indeed, previous studies have incorporated the textured-induced magnetic and electric fields and shown that this gives raise to the so-called topological torque and topological damping that directly influence the mobility of skyrmions [60, 61].

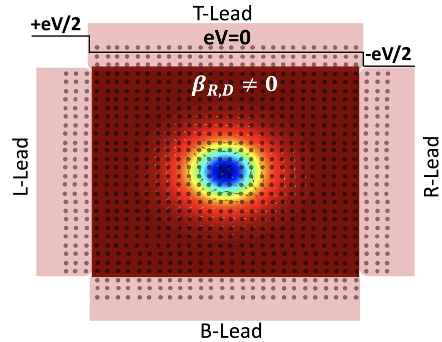

FIG. 4. Schematic diagram of four-terminal setup made up of a central region containing a magnetic skyrmion in the presence of SOC attached to four ferromagnetic leads L, T, R, B. The system is subjected to a longitudinal voltage bias of eV while the transverse leads measure the Hall respond of the system.

IV. NUMERICAL RESULTS

We corroborate our analytical predictions via numerical calculations of the THE of electrons as they traverse an isolated skyrmion in the presence of RSOC or DSOC. Our considerations are based on a two-dimensional tight-binding model on a square lattice, described by the Hamiltonian

$$\mathcal{H} = \sum_{\boldsymbol{i}} \hat{c}^\dagger_{\boldsymbol{i}}\big(\epsilon_{\boldsymbol{i}} + J\boldsymbol{m}_{\boldsymbol{i}}\cdot\hat{\boldsymbol{\sigma}}\big)\hat{c}_{\boldsymbol{i}} - \sum_{<\boldsymbol{i},\boldsymbol{j}>} \hat{c}^\dagger_{\boldsymbol{i}} t_{\boldsymbol{ij}}\hat{c}_{\boldsymbol{j}}, \tag{13}$$

where $\epsilon_{\boldsymbol{i}}$ and $\hat{c}^\dagger_{\boldsymbol{i}}(\hat{c}_{\boldsymbol{i}})$ are the onsite energy and the spinor creation (annihilation) operators on site $\boldsymbol{i} = (i_x, i_y)$, respectively. J is the exchange energy that couples the spin of electrons $\hat{\boldsymbol{\sigma}}$ to local magnetization $\boldsymbol{m}_{\boldsymbol{i}}$, and $t_{\boldsymbol{ij}}$ is the nearest-neighbor hopping that incorporates the spin-orbit interaction and is given by

$$t_{\boldsymbol{ij}} = \begin{cases} t_0 + it_R\sigma_y + it_D\sigma_x, & \boldsymbol{j} = \boldsymbol{i} \pm (1,0), \\ t_0 - it_R\sigma_x - it_D\sigma_y, & \boldsymbol{j} = \boldsymbol{i} \pm (0,1). \end{cases} \tag{14}$$

Here t_0 is the hopping in the absence of SOC, $t_{R(D)} = \beta_{R(D)}/a_0$ and a_0 is the lattice constant. We note that at low band filling, there is direct correspondence between the continuous and discrete Hamiltonians given in Eq. (1) and Eq. (13), respectively for $t_0 = \hbar^2/2m^* a_0^2$ [62]. An isolated skyrmion of radius $r_s = 10a_0$ in embedded in a ferromagnetic background to which four ferromagnetic leads are attached as depicted in Fig. 4. We employ the Landauer-Büttiker formalism [63] to investigate the coherent charge transport in our system which we subject to a longitudinal bias voltage across the left (L) and right (R) leads and measure the transverse responds via the top (T) and bottom (B) leads. The terminal current of the μ-lead is calculated as

$$I_\mu = \frac{e^2}{2\pi\hbar} \sum_{\mu \neq \nu} (T_{\nu\mu} V_\mu - T_{\mu\nu} V_\nu), \tag{15}$$

where V_μ is the voltage at the μ-lead and $T_{\nu\mu}$ is the transmission coefficient for electrons from the μ-lead to the ν-lead, which is calculated via the use of the KWANT software package [64]. The terminal voltages are calculated following Ref. 46, from which the THE is quantified via the topological Hall angle defined as

$$\theta_{\mathrm{TH}} = \frac{V_T - V_B}{V_R - V_L}. \tag{16}$$

We consider the strong exchange limit with $J = 5t_0$, and investigate the dependence of θ_{TH} on the strength of RSOC (t_R) for Néel-type and DSOC (t_D) for Bloch-type skyrmions and antiskyrmions. Furthermore, to rule out any possibility that our results stem from size-effect, we perform a systematic study with different system sizes $L \times L$, for $L = 101a_0$, $161a_0$, $181a_0$ and an optimal (to ensure smooth enough magnetization variation from system to leads [61]) skyrmion radius of $10a_0$. Our numerical results as shown in Fig. 5, confirm the physics underscored by our analytical derivations i.e., the existence an optimal strength of RSOC (DSOC) at which the the topological Hall effect vanishes in Néel-skyrmions (Bloch antiskyrmions). Furthermore, the green arrow in Figs. 5 (a) and (b) shows that the value of t_R for Néel skyrmion and t_D for Bloch antiskyrmion at which the THE vanishes (green arrow) is independent on the system size as such, we rule out the possibilities that the observe results are artifact from size effect.

Finally, based on our analytical prediction given by Eq. (12), the estimate for the strength of the RSOC/DSOC at which the THE vanishes ($t^*_{R(D)}$) for a skyrmion of radius $r_s = 10a_0$ is predicted to be $t^*_{R/D} = 0.2t_0$. This value is very close to what we obtained numerically ($t^*_{R/D} = 0.17t_0$) using similar sets of parameters. We attribute the small discrepancy to nonlinear corrections, and most importantly, to the fact that our model does not take into account the explicit dependence of the skyrmion size on the SOC. The latter which is out of the scope of this work, can be investigated via, for example using micro-magnetic simulations.

We conclude this study by investigating the effect of disorder which are unavoidable in real materials. We model nonmagnetic impurity scattering via the randomization of the onsite energy given in Eq. (13) i.e., $\epsilon_{\boldsymbol{i}} \to \epsilon_{\boldsymbol{i}} + \delta V_{\boldsymbol{i}}$, where $\delta V_{\boldsymbol{i}} \in [-(W/2), (W/2)]$, with W being the strength of the disorder and taking average over 50,000 disorder configurations. We calculated the THE in the presence of nonmagnetic impurity scattering for different impurity strength for which the transport of electrons remains adiabatic (the adiabaticity condition might be lost in the diffusive regime), since our analysis is based on the adiabatic limit of the spin of electrons following the direction of the local magnetization. Our result as depicted in Fig. 5 (c) shows that for impurity strength of $W = 0.5t_0, 0.75t_0, 1.0t_0$ and $1.25t_0$ which correspond to mean-free-path (λ) of $\lambda = 140a_0, 66a_0, 38a_0$ and $21a_0$, respectively, disorder scattering does not affect our conclusions in the preceding section. Therefore, our proposal

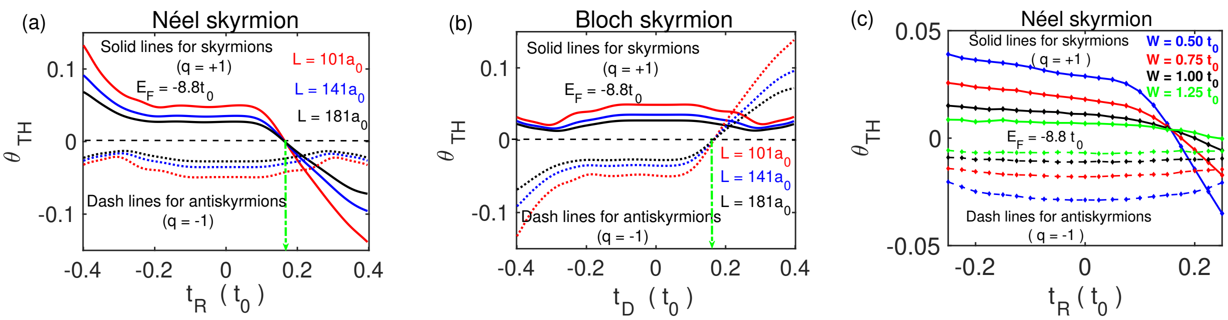

FIG. 5. Dependence of the THE on the strength of (a) RSOC (t_R) for Néel and (b) DSOC (t_D) for Bloch skyrmion and antiskyrmion, for different system sizes. Notice that the value of t_R for Néel skyrmion and t_D for Bloch antiskyrmion at which the THE vanishes is independent on the system size. (c) Dependence of THE on t_R for different impurity strengths for Néel skyrmion and antiskyrmion.

of tuning the THE in magnetic solitons is robust against impurity scattering provided that transport of electrons remains adiabatic.

V. CONCLUSIONS

Magnetic skyrmions are hugely considered as a contender for information carriers in future spintronic applications. However, the parasitic SkHE constitutes a technological challenge for the integration of the former in such applications. Several theoretical proposals, which focus on suppressing the Magnus force that gives raise to this detrimental SkHE, have been put forward. In this study, we focus on exploring the possibilities of overcoming the SkHE via tuning spin-orbit interactions that are inherent in skyrmionic systems. Starting from the emergent electrodynamics in the latter in the presence of SOC, we demonstrate that the additional SOC-induced emergent fictitious magnetic fields can be used to tune the SkHE. Our calculations show that by tuning the strength of RSOC in Néel skyrmions or DSOC in Bloch antiskyrmions, it is possible to achieve a current-driven motion without SkHE in these systems. Our findings open up promising perspective on overcoming the SkHE.

C. A. A. thanks M. Ishida for technical assistance and A. Abbout for stimulating discussions. This work was supported by Grant-in-Aid for Exploratory Research (No. 16K13853) and Grant-in-Aid for Scientific Research (B) (No. 17H02929) from Japan Society for the Promotion of Science (JSPS). H. L. acknowledges support from HeNan University (Grant No. CJ3050A0240050) and National Natural Science Foundation of China (Grants No. 11804078). O. A. T. acknowledges support by the Cooperative Research Project Program at the Research Institute of Electrical Communication, Tohoku University and by UNSW Science International Seed grant.

[1] A. Manchon, A new moment for Berry, Nat. Phys. **10**, 340 (2014).

[2] T. Kuschel and G. Reiss, Charges ride the spin wave, Nat. Nanotechnol. **10**, 22 (2015).

[3] G. Chen, Skyrmion Hall effect, Nat. Phys. **13**, 112 (2017).

[4] J. Sinova, S. O. Valenzuela, J. Wunderlich, C. H. Back, and T. Jungwirth, Spin Hall effects, Rev. Mod. Phys. **87**, 1213 (2015).

[5] A. Hoffmann and S. D. Bader, Opportunities at the Frontiers of Spintronics, Phys. Rev. Applied **4**, 047001 (2015).

[6] T. Moriya, Anisotropic Superexchange Interaction and Weak Ferromagnetism, Phys. Rev. **120**, 91 (1960).

[7] I. Dzyaloshinsky, A thermodynamic theory of "weak" ferromagnetism of antiferromagnetics, J. Phys. Chem. Solids **4** 241 (1958).

[8] J. Kishine and A. Ovchinnikov, Theory of Monoaxial Chiral Helimagnet, Solid State Phys. **66**, 1 (2015).

[9] U. K. Rößler, A. N. Bogdanov, and C. Pfleiderer, Spontaneous skyrmion ground states in magnetic metals, Nature **442**, 797 (2006).

[10] N. Nagaosa, and Y. Tokura, Topological properties and dynamics of magnetic skyrmions, Nat. Nanotechnol. 8, 899 (2013).

[11] A. Fert, V. Cros, and J. Sampaio, Skyrmions on the track, Nat. Nanotechnol. **8**, 152 (2013).

[12] K. Litzius, I. Lemesh, B. Krüger, P. Bassirian, L. Caretta, K. Richter, F. Büttner, K. Sato, O. A. Tretiakov, J. Förster, R. M. Reeve, M. Weigand, I. Bykova, H. Stoll, G. Schütz, G. S. D. Beach, and M. Kläui, Skyrmion Hall effect revealed by direct time-resolved X-ray microscopy, Nat. Phys. **13**, 170 (2017).

[13] W. Jiang, X. Zhang, G. Yu, W. Zhang, X. Wang, M. B. Jungfleisch, J. E. Pearson, X. Cheng, O. Heinonen, K. L. Wang, Y. Zhou, A. Hoffmann, and S. G. E. te Velthuis, Direct observation of the skyrmion Hall effect, Nat. Phys. **13**, 162 (2017).

[14] J. Barker and O. A. Tretiakov, Static and Dynamical Properties of Antiferromagnetic Skyrmions in the Presence of Applied Current and Temperature, Phys. Rev. Lett. **116**, 147203 (2016).

[15] X. Zhang, Y. Zhou, and M. Ezawa, Antiferromagnetic Skyrmion: Stability, Creation and Manipulation, Sci. Rep. **6**, 24795 (2016).

[16] B. Göbel, A. Mook, J. Henk, and I. Mertig, Antiferromagnetic skyrmion crystals: Generation, topological Hall, and topological spin Hall effect, Phys. Rev. B **96**, 060406(R) (2017).

[17] C. A. Akosa, O. A. Tretiakov, G. Tatara, and A. Manchon, Theory of the Topological Spin Hall Effect in Antiferromagnetic Skyrmions: Impact on Current-Induced Motion, Phys. Rev. Lett. **121**, 097204 (2018).

[18] Y. Zhang, S. Luo, B. Yan, J. O-Yang, X. Yang, S. Chen, B. Zhu, and L. You, Magnetic skyrmions without the skyrmion Hall effect in a magnetic nanotrack with perpendicular anisotropy, Nanoscale **9**, 10212 (2017).

[19] X. Zhang, Y. Zhou, and M. Ezawa, Magnetic bilayer-skyrmions without skyrmion Hall effect, Nat. Commun. **7** 10293 (2016).

[20] M. Finazzi, M. Savoini, A. R. Khorsand, A. Tsukamoto, A. Itoh, L. Duò, A. Kirilyuk, Th. Rasing, and M. Ezawa, Laser-Induced Magnetic Nanostructures with Tunable Topological Properties, Phys. Rev. Lett. **110**, 177205 (2013).

[21] F. Zheng, H. Li, S. Wang, D. Song, C. Jin, W. Wei, A. Kovács, J. Zang, M. Tian, Y. Zhang, H. Du, and R. E. Dunin-Borkowski, Direct Imaging of a Zero-Field Target Skyrmion and Its Polarity Switch in a Chiral Magnetic Nanodisk, Phys. Rev. Lett. **119**, 197205 (2017).

[22] S. Zhang, F. Kronast, G. van der Laan, and T. Hesjedal, Real-Space Observation of Skyrmionium in a Ferromagnet-Magnetic Topological Insulator Heterostructure, Nano Lett. **18**, 1057 (2018).

[23] M. Beg, R. Carey, W. Wang, D. Cortés-Ortuño, M. Vousden, M.-A. Bisotti, M. Albert, D. Chernyshenko, O. Hovorka, R. L. Stamps, and H. Fangohr, Ground state search, hysteretic behaviour, and reversal mechanism of skyrmionic textures in confined helimagnetic nanostructures, Sci. Rep. **5**, 17137 (2015).

[24] M. Beg, M. Albert, M.-A. Bisotti, D. Cortés-Ortuño, W. Wang, R. Carey, M. Vousden, O. Hovorka, C. Ciccarelli, C. S. Spencer, C. H. Marrows, and H. Fangohr, Dynamics of skyrmionic states in confined helimagnetic nanostructures, Phys. Rev. B **95**, 014433 (2017).

[25] X. Zhang, J. Xia, Y. Zhou, D. Wang, X. Liu, W. Zhao, and M. Ezawa, Control and manip-

ulation of a magnetic skyrmionium in nanostructures, Phys. Rev. B **94**, 094420 (2016).

[26] S. Huang, C. Zhou, G. Chen, H. Shen, A. K. Schmid, K. Liu, and Y. Wu, Stabilization and current-induced motion of antiskyrmion in the presence of anisotropic Dzyaloshinskii-Moriya interaction, Phys. Rev. B **96**, 144412 (2017).

[27] M. N. Potkina, I. S. Lobanov, O. A. Tretiakov, H. Jónsson, and V. M. Uzdin, Antiskyrmions in Ferromagnets and Antiferromagnets: Stability and Dynamics, arXiv:1906.06383 (2019).

[28] B. Göbel, A. Mook, J. Henk, and I. Mertig, Overcoming the speed limit in skyrmion racetrack devices by suppressing the skyrmion Hall effect, Phys. Rev. B **99**, 020405(R) (2019).

[29] S. E. Barnes and S. Maekawa, Generalization of Faraday's Law to Include Nonconservative Spin Forces, Phys. Rev. Lett. **98**, 246601 (2007).

[30] A. Neubauer, C. Pfleiderer, B. Binz, A. Rosch, R. Ritz, P. G. Niklowitz, and P. Böni, Topological Hall Effect in the A Phase of MnSi, Phys. Rev. Lett. **102**, 186602 (2009).

[31] T. Schulz, R. Ritz, A. Bauer, M. Halder, M. Wagner, C. Franz, C. Pfleiderer, K. Everschor, M. Garst, and A. Rosch, Emergent electrodynamics of skyrmions in a chiral magnet, Nat. Phys. **8**, 301 (2012).

[32] N. Nakabayashi, and G. Tatara, Rashba-induced spin electromagnetic fields in the strong sd coupling regime, New J. Phys. **16**, 015016 (2014).

[33] K.-W. Kim, J.-H. Moon, K.-J. Lee, and H.-W. Lee, Prediction of Giant Spin Motive Force due to Rashba Spin-Orbit Coupling, Phys. Rev. Lett. **108**, 217202 (2012).

[34] G. Tatara, N. Nakabayashi, and K.-J. Lee, Spin motive force induced by Rashba interaction in the strong *sd* coupling regime, Phys. Rev. B **87**, 054403 (2013).

[35] G. Tatara, H. Kohno, J. Shibata, Y. Lemaho, and K.-J. Lee, Spin Torque and Force due to Current for General Spin Textures, J. Phys. Soc. Jpn. **76**, 054707 (2007).

[36] C. A. Akosa, A. Takeuchi, Z. Yuan, and G. Tatara, Theory of chiral effects in magnetic textures with spin-orbit coupling, Phys. Rev. B **98**, 184424 (2018).

[37] R. Winkler, Spin-Orbit Coupling Effects in Two-Dimensional Electron and Hole Systems, Vol. **191** (Springer Tracts in Modern Physics, 2003).

[38] K. Premasiri and X. P. A. Gao, Tuning spin-orbit coupling in 2D materials for spintronics: a topical review, J. Phys.: Condens. Matter **31**, 193001(2019).

[39] S. Mühlbauer, B. Binz, F. Jonietz, C. Pfleiderer, A. Rosch, A. Neubauer, R. Georgii, and P. Böni, Skyrmion Lattice in a Chiral Magnet, Science **323**, 915 (2009).

[40] X. Z. Yu, Y. Onose, N. Kanazawa, J. H. Park, J. H. Han, Y. Matsui, N. Nagaosa, and Y. Tokura, Real-space observation of a two-dimensional skyrmion crystal, Nature (London) **465**, 901 (2010).

[41] S. Seki, X. Yu, S. Ishiwata, and Y. Tokura, Observation of Skyrmions in a Multiferroic Material, Science **336**, 198 (2012).

[42] I. Kézsmárki, S. Bordács, P. Milde, E. Neuber, L. M. Eng, J. S. White, H. M. Rønnow, C. D. Dewhurst, M. Mochizuki, K. Yanai, H. Nakamura, D. Ehlers, V. Tsurkan, and A. Loidl, Néel-type skyrmion lattice with confined orientation in the polar magnetic semiconductor GaV_4S_8, Nat. Mater. **14**, 1116 (2015).

[43] T. Kurumaji, T. Nakajima, V. Ukleev, A. Feoktystov, T. Arima, K. Kakurai, and Y. Tokura, Néel-Type Skyrmion Lattice in the Tetragonal Polar Magnet $VOSe_2O_5$, Phys. Rev. Lett. **119**, 237201 (2017).

[44] S. Hayami and Y. Motome, Néel- and Bloch-Type Magnetic Vortices in Rashba Metals, Phys. Rev. Lett. 121, 137202 (2018).

[45] J. Rowland, S. Banerjee, and M. Randeria, Skyrmions in chiral magnets with Rashba and Dresselhaus spin-orbit coupling, Phys. Rev. B **93**, 020404(R) (2016).

[46] P. B. Ndiaye, C. A. Akosa, and A. Manchon, Topological Hall and spin Hall effects in disordered skyrmionic textures, Phys. Rev. B **95**, 064426 (2017).

[47] O. A. Tretiakov and O. Tchernyshyov, Vortices in thin ferromagnetic films and the skyrmion number, Physical Review B **75**, 012408 (2007).

[48] G. Tatara, and H. Fukuyama, Macroscopic quantum tunneling of a domain wall in a ferromagnetic metal, Phys. Rev. Lett. **72** 772 (1994).

[49] G. Tatara, and H. Fukuyama, Macroscopic Quantum Tunneling of a Domain Wall in a Ferromagnetic Metal, J. Phys. Soc. Jpn. **63** 2538 (1994).

[50] K. S. Denisov, I. V. Rozhansky, S. Averkiev, and E. Lähderanta, Electron Scattering on a Magnetic Skyrmion in the Nonadiabatic Approximation Phys. Rev. Lett. **117**, 027202 (2016).

[51] K. S. Denisov, I. V. Rozhansky, S. Averkiev, and E. Lähderanta, General theory of the topological Hall effect in systems with chiral spin textures, Phys. Rev. B **98**, 195439 (2018).

[52] K. Nakazawa, M. Bibes, and H. Kohno, Topological Hall Effect from Strong to Weak Coupling, J. Phys. Soc. Jpn. **87**, 033705 (2018).

[53] K. Nakazawa and H. Kohno, Weak coupling theory of topological Hall effect Phys. Rev. B **99**, 174425 (2019).

[54] L. N. Oveshnikov, V. A. Kulbachinskii, A. B. Davydov, B. A. Aronzon, I. V. Rozhansky, N. S. Averkiev, K. I. Kugel, and V. Tripathi, Berry phase mechanism of the anomalous Hall effect in a disordered two-dimensional magnetic semiconductor structure, Sci. Rep. **5**, 17158 (2015).

[55] K.-W. Kim, H.-W. Lee, K.-J. Lee, and M. D. Stiles, Chirality from Interfacial Spin-Orbit Coupling Effects in Magnetic Bilayers, Phys. Rev. Lett. **111**, 216601 (2013).

[56] N. S. Kiselev, A. N. Bogdanov, R. Schäfer, and U. K. Rössler, Chiral skyrmions in thin magnetic films: new objects for magnetic storage technologies?, J. Phys. D: Appl. Phys. **44**, 392001 (2011).

[57] S. Rohart, and A. Thiaville, Skyrmion confinement in ultrathin film nanostructures in the presence of Dzyaloshinskii-Moriya interaction, Phys. Rev. B **88**, 184422 (2013).

[58] T. Kikuchi, T. Koretsune, R. Arita, and G. Tatara, Dzyaloshinskii-Moriya Interaction as a Consequence of a Doppler Shift due to Spin-Orbit-Induced Intrinsic Spin Current Phys. Rev. Lett. **116**, 247201 (2016).

[59] T. Koretsune, T. Kikuchi, and R. Arita, First-Principles Evaluation of the Dzyaloshinskii-Moriya Interaction, J. Phys. Soc. Jpn. **87**, 041011 (2018).

[60] A. Bisig, C. A. Akosa, J.-H. Moon, J. Rhensius, C. Moutafis, A. v. Bieren, J. Heidler, G. Kiliani, M. Kammerer, M. Curcic, M. Weigand, T. Tyliszczak, B. V. Waeyenberge, H. Stoll, G. Schütz, K.-J. Lee, A.n Manchon, and M. Kläui, Enhanced Nonadiabaticity in Vortex Cores due to the Emergent Hall Effect, Phys. Rev. Lett. **117**, 277203 (2016).

[61] C. A. Akosa, P. B. Ndiaye, and A. Manchon, Intrinsic nonadiabatic topological torque in magnetic skyrmions and vortices, Phys. Rev. B **95**, 054434 (2017).

[62] B. K. Nikolić, S. Souma, L. P. Zârbo, and J. Sinova, Nonequilibrium Spin Hall Accumulation in Ballistic Semiconductor Nanostructures, Phys. Rev. Lett. **95**, 046601 (2005).

[63] M. Büttiker, Four-Terminal Phase-Coherent Conductance, Phys. Rev. Lett. **57**, 1761 (1986).

[64] C. W. Groth, M. Wimmer, A. R. Akhmerov, X. Waintal, Kwant: a software package for quantum transport, New J. Phys. **16**, 063065 (2014).